Nanoscale

PAPER

View Article Online
View Journal | View Issue

Cite this: *Nanoscale*, 2016, **8**, 11084

A facile one-step solution deposition *via* non-solvent/solvent mixture for efficient organometal halide perovskite light-emitting diodes†

Bo Jiao,‡ Xiaobo Zhu, Wen Wu, Hua Dong, Bin Xia, Jun Xi, Ting Lei, Xun Hou and Zhaoxin Wu*‡

Received 6th February 2016,
Accepted 21st April 2016

DOI: 10.1039/c6nr01092j

www.rsc.org/nanoscale

Although organometal halide perovskite materials have shown great potential in light-emitting diodes, their performance is greatly restricted by the poor morphology of the perovskite layer. In this work, we demonstrate a facile one-step solution method to improve the perovskite film morphology *via* a non-solvent/solvent mixture. An efficient $CH_3NH_3PbBr_3$-based light-emitting diode was prepared with a chlorobenzene/*N*,*N*-dimethylformamide mixed solvent. A high efficiency of 0.54 cd A^{-1} is demonstrated, which is 22 times higher than that of a device fabricated by a traditional one-step solution process. Furthermore, the uniformity of the emission region and the device stability are strongly improved by this facile one-step solution process. Our work paves a new way for the morphological control of perovskite films for application in light-emitting diodes.

Introduction

The organometal halide perovskite materials have attracted considerable interest because of their exceptional optoelectronic properties,[1,2] such as their high mobility of ambipolar carrier transport,[3] high photoluminescence quantum efficiency,[4] tuneable optical bandgap from the visible to infrared region[5] and long-range charge carrier diffusion length.[6] Moreover, perovskite materials with high crystallinity can be solution-processed easily at low temperature, which makes them very attractive materials for low-cost and large-area optoelectronic applications. At the end of the past century, a lot of effort was put into the development of light-emitting diodes based on organometal halide perovskite materials.[7,8] However, electroluminescence was only demonstrated at very low temperature (~77 K). Recently, intensive work has been dedicated to the research of methylammonium lead halide perovskite ($CH_3NH_3PbX_3$, X = I, Br, Cl) materials due to their enormous potentiality for photovoltaic applications,[9–11] which has successfully awakened interest for using them as light emitters. Very recently, bright and colour-controlled electroluminescence at room temperature was demonstrated in these methylammonium lead halide perovskite light-emitting diodes (PeLEDs),[5,12–19] thereby opening up a potential range of display and lighting applications for these materials.

The poor coverage of perovskite films, which leads to seriously non-radiative leakage current losses, is still one of the bottlenecks for improving the performance of PeLEDs. To suppress the leakage current in PeLEDs, different methods have been demonstrated, which can be generally split into two approaches. One is to control the formation process of the perovskite film to achieve a uniform and smooth surface by an interfacial treatment method, such as the use of an ultrathin polyethyleneimine (PEI) modification layer,[15] by interfacial treatment with a polar solvent[14] or by interfacial treatment with a highly volatile non-polar solvent.[19] These interfacial treatments, however, are complex and delicate, which limits the repeatability of the fabrication process of the perovskite film. Another is to block the film's pinholes by a dielectric polymer, such as a polyimide precursor dielectric (PIP),[18] which is an effective way to suppress the non-radiative current loss. However, the dielectric polymer is harmful to the electrical properties of PeLEDs. Therefore, how to prepare smooth perovskite films with full coverage is still a pivotal issue for the construction of PeLED devices with superior performance.

In this work, we report an improved one-step solution process using a non-solvent/solvent mixture for efficient PeLEDs. $MAPbBr_3$ (MA = CH_3NH_3), which exhibits a high air

Key Laboratory for Physical Electronics and Devices of the Ministry of Education & Shannxi Key Lab of Information Photonic Technique, School of Electronic and Information Engineering, Xi'an Jiaotong University, No. 28, Xianning West Road, Xi'an, 710049, China. E-mail: zhaoxinwu@mail.xjtu.edu.cn

† Electronic supplementary information (ESI) available: MABr/PbBr ratio optimization, film thickness and AFM morphology. See DOI: 10.1039/c6nr01092j

‡ These authors equally contributed to this work.

stability and exciton binding energy (~84 meV),[20] is used as the green emission layer. The mixed solvent is constituted by chlorobenzene (CBZ), which is a typical non-solvent of the $MAPbBr_3$ precursor (*i.e.* MABr and $PbBr_2$), and a good solvent of the $MAPbBr_3$ precursor, *N*,*N*-dimethylformamide (DMF).[10] Based on this improved one-step solution process, a maximum luminance of 3868 cd m^{-2} and a current efficiency of 0.54 cd A^{-1} were demonstrated, which represents a more than 20-fold improvement over the values for a control device fabricated by a traditional one-step solution process. Furthermore, it was also demonstrated that our approach can significantly enhance the uniformity of the emission region as well as the device stability.

Experimental

MABr was synthesized and purified according to a previous report.[5] After that, a 20 wt% $MAPbBr_3$ solution was prepared by reacting MABr and $PbBr_2$ (Aldrich) in a mixed solvent at 60 °C for 2 hours. The optimized molar ratio of MABr : $PbBr_2$ is 1.5 : 1 (see Fig. S1, ESI†). The volume ratios of CBZ to DMF in the mixed solvent were 1/10, 2/10, 3/10 and 4/10, respectively. To compare the influence of the solution concentration on the film morphology, a 5 wt% $MAPbBr_3$ solution using a 4/10 CBZ/DMF mixed solvent was prepared. A 20 wt% $MAPbBr_3$ solution using traditional DMF solvent was also prepared for control device fabrication. The film thickness was determined by a Dektak profilometer. It was found that all film thicknesses were around 140 nm, except the film fabricated by the 5 wt% $MAPbBr_3$ solution, the thickness of which was around 48 nm (see Fig. S2, ESI†). The equilibrium solubility of the $MAPbBr_3$ precursor in different solutions was measured by the widely used saturation shake-flask method that is the same as described in a previous report.[21]

Indium tin oxide (ITO) glass with a sheet resistance of 25 Ω $\square^{-1}$ was used as the substrate. Prior to device fabrication, ITO substrates were cleaned with deionized water and organic solvents and then exposed to a UV-ozone atmosphere for 5 minutes. Then, a 40 nm-thick PEDOT:PSS (AI4083 CLEVIOS) layer was deposited by spin-coating. The PEDOT:PSS film was then baked at 120 °C for 20 minutes in air. After the film had cooled down, the $MAPbBr_3$ precursor was spin-coated on the PEDOT:PSS layer at 3000 rpm, and then baked at 80 °C for 15 minutes in a glove box with a N_2 atmosphere. Then, the $MAPbBr_3$ film was transported into a thermal evaporation chamber without air exposure for the fabrication of an organic layer, as well as the LiF/Al cathode. The base pressure during the evaporation process was about 1×10^{-3} Pa. The evaporation rates for the organic layer, LiF and Al were 0.3 nm s^{-1}, 0.1 nm s^{-1} and 1 nm s^{-1}, respectively. The thickness of the films was determined *in situ* by a quartz crystal sensor and *ex situ* by a profilometer. The emission area of the device was about 12 mm^2. Luminance–current–voltage (*L*–*I*–*V*) characteristics, as well as the stability performance of the devices, were measured using a computer-controlled sourcemeter (Keithley 2602) and a calibrated silicon photodiode. All measurements were carried out at room temperature in the glove box in a 99.999% N_2 atmosphere to exclude the influence of an air atmosphere on the device performance.[17] Electroluminescence spectra were measured using a PR650 spectrometer. The surface morphology was investigated by scanning electron microscopy (SEM), atomic-force microscopy (AFM, Bruker) and a 50× microscope objective with a numerical aperture of 0.5 (Nikon, Japan). The perovskite film was characterized by X-ray diffraction (XRD) (D/MAX-2400, Rigaku, Japan) with Cu Kα radiation. Photoluminescence spectra of the perovskite films were recorded using a fluorescence spectrophotometer (Fluoromax 4, HORIBA Jobin Yvon). Time-resolved PL spectra were recorded with a 100 ps time resolution using a time-correlated single photon counting (TCSPC) system (FLS920 spectrometer) (excited by picosecond pulsed LEDs, pulse duration: <850 ps, repetition rate: 10 MHz).

Results and discussion

The influence of the CBZ/DMF ratio on the $MAPbBr_3$ film morphology is shown in Fig. 1(a)–(e). As shown in Fig. 1(a), an iso-

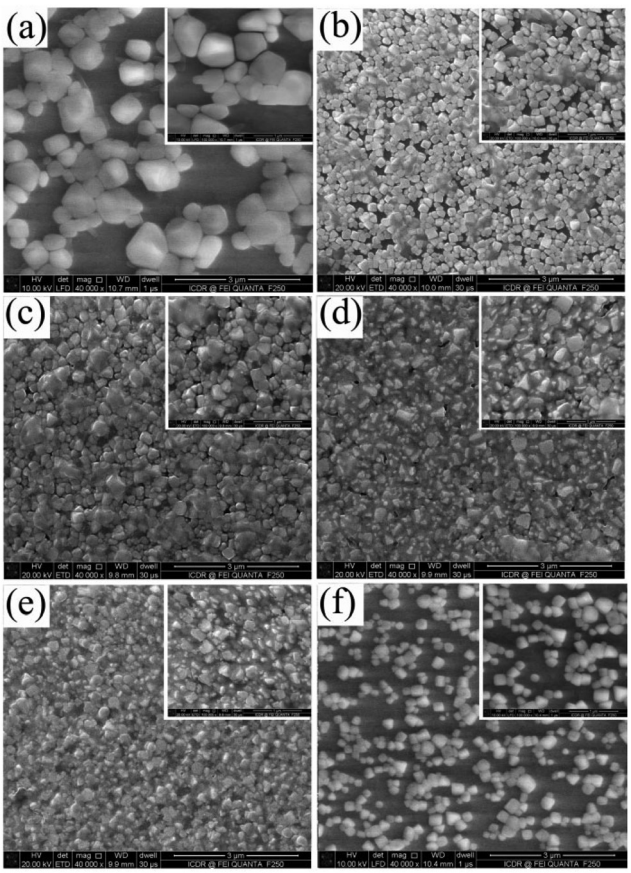

Fig. 1 Top-view SEM images of $MAPbBr_3$ films deposited on PEDOT:PSS/ITO substrates. The $MAPbBr_3$ films were fabricated using solutions with different CBZ/DMF ratios of 0/1 (a), 1/10 (b), 2/10 (c), 3/10 (d), 4/10 (e) and 4/10 (f), respectively. The concentrations of the solutions used for (a)–(e) were 20 wt%, and that of the solution used for (f) was 5 wt%. The insets show images with higher resolution.

lated crystalline layer with grain size ~1 μm was formed by the $MAPbBr_3$ solution using DMF solvent. The film coverage was rather low, at ~54% (estimated from SEM images using the software ImageJ). When the CBZ was added into the solvent, the $MAPbBr_3$ grain size decreased dramatically. As shown in Fig. 1(b), the grain size of a film fabricated using a 1/10 CBZ/DMF solvent was in the range from 100 nm to 300 nm. With an increase in the proportion of CBZ in the mixed solvent, however, the crystal size of the $MAPbBr_3$ did not decrease further, as is shown in Fig. 1(c)–(e). Furthermore, the coverage of the $MAPbBr_3$ films was significantly enhanced by increasing the proportion of CBZ. As shown in Fig. 1(b)–(e), the coverage percentages of $MAPbBr_3$ films fabricated with different CBZ/DMF ratios of 1/10, 2/10, 3/10 and 4/10 were ~88%, ~92%, ~95% and ~98%, respectively, which indicates an increase in the crystal density. A film was also prepared using a $MAPbBr_3$ solution of low concentration (5 wt%, 4/10 CBZ/DMF) to check the influence of solution concentration, as shown in Fig. 1(f). In the low concentration situation, the CBZ addition also suppressed the formation of large isolated cuboid $MAPbBr_3$ nanocrystals. However, because of the low solution concentration, the coverage of this layer was still poor, at ~45%, which indicates that the solution concentration is also important for a high coverage film. The film roughness can also be improved by using a CBZ/DMF solvent. According to the AFM test, the root mean squared (RMS) values for the different films were 76.0 nm (pure DMF, 20 wt%), 43.1 nm (1/10 CBZ/DMF, 20 wt%), 37.1 nm (2/10 CBZ/DMF, 20 wt%), 36.4 nm (3/10 CBZ/DMF, 20 wt%), 28.3 nm (4/10 CBZ/DMF, 20 wt%) and 33.1 nm (4/10 CBZ/DMF, 5 wt%), respectively (see Fig. S3, ESI†). The films fabricated using the mixed solvent were significantly smoother than that fabricated using DMF.

The crystallinity of the $MAPbBr_3$ films mentioned above was also characterized by XRD. As shown in Fig. 2, the $MAPbBr_3$ films fabricated by 20 wt% solutions gave diffraction peaks at 14.90°, 20.99°, 30.03° and 43.1°, which are assigned to the (100), (110), (200) and (220) planes of a cubic perovskite structure, respectively.[9,24] However, only one peak, located at 14.92°, could be observed for the $MAPbBr_3$ film fabricated using the 5 wt% solution, because of its thin thickness.

The improvement of the film morphology can be attributed to the influence of the mixed solvent on the nucleation process in the film formation. Generally, the crystallization process consists of nucleation and growth stages. Nucleation rate, *i.e.* the number of nuclei formed per unit of volume and time, is a crucial parameter to describe the nucleation process. In the classical nucleation theory, the nucleation rate (J) is given by the following expression:[22]

$$J \propto \exp\left[\frac{-B\sigma^3\Omega^2}{k^3T^3(\ln S)^2}\right], \quad (1)$$

where B is a shape factor, σ is the interfacial free energy, Ω is the molecular volume, k is the Boltzmann constant and T is the absolute temperature; S is the supersaturation, which can be presented in the following form:[22,23]

$$S = \frac{C}{C_e}, \quad (2)$$

where C is the actual concentration of the solution and C_e is the equilibrium solubility. From the expressions (1) and (2), it is clear that the nucleation rate is a very sharp function of the supersaturation, and that the supersaturation can be further influenced by the solution solubility (C_e) and the solution concentration (C). The decrease of the solution solubility increases the nucleation rate in the crystallization process. For each spin-coating process, the amount of $MAPbBr_3$ can be considered as constant. Thus, the larger the nucleation rate is, the smaller the grain size of the $MAPbBr_3$ film is. Fig. 3 shows the solubility of the $MAPbBr_3$ precursors, *i.e.* $PbBr_2$ and MABr, as a function of the DMF/CBZ ratio. As shown in Fig. 3, the solubility of the $MAPbBr_3$ precursors is strongly dependent on the CBZ/DMF ratio. With the increasing of the proportion of CBZ in the mixed solvent, both the solubility of $PbBr_2$ and that of

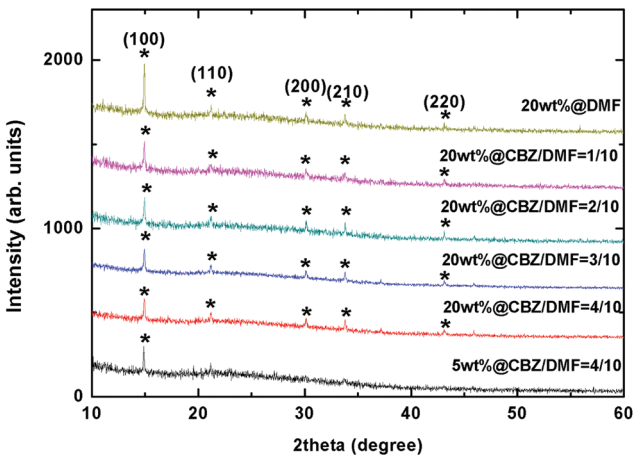

Fig. 2 XRD patterns of the $MAPbBr_3$ films fabricated by solutions with different CBZ/DMF ratios, as well as different solution concentrations.

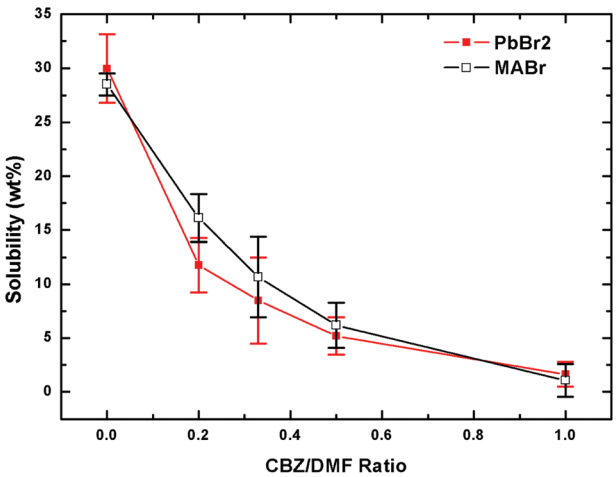

Fig. 3 Solubilities of the $PbBr_2$ and the MABr in solvents with CBZ/DMF ratios of 0/1, 1/5, 1/3, 1/2 and 1/1 at T = 298 K.

MABr decreases dramatically. Thus, the $MAPbBr_3$ grain size becomes smaller when the mixed solvent is used, which coincides with the experimental results.

$MAPbBr_3$-based PeLEDs using the improved one-step solution process *via* a non-solvent/solvent mixture were fabricated with a structure of ITO/PEDOT:PSS (40 nm)/$MAPbBr_3$/bathophenanthroline (Bphen) (60 nm)/LiF (1 nm)/Al (100 nm). Here, Bphen was used as an electron transporting layer as well as a hole blocking layer due to the large barrier between the ionization potential level of $MAPbBr_3$ and the highest occupied molecular orbital level of Bphen, just as shown in the inset of Fig. 4(a). To examine the influence of the CBZ/DMF ratio as well as the solution concentration on the performance of the PeLEDs, the $MAPbBr_3$ layer was fabricated using 20 wt% $MAPbBr_3$/DMF solution, 20 wt% $MAPbBr_3$/(CBZ/DMF = 1/10) solution, 20 wt% $MAPbBr_3$/(CBZ/DMF = 2/10) solution, 20 wt% $MAPbBr_3$/(CBZ/DMF = 3/10) solution, 20 wt% $MAPbBr_3$/(CBZ/DMF = 4/10) solution and 5 wt% $MAPbBr_3$/(CBZ/DMF = 4/10) solution, respectively.

Fig. 4(a) and (b) present the current density *versus* voltage (*J*–*V*) and luminance *versus* voltage (*L*–*V*) characteristics of these PeLEDs. As shown in Fig. 4(a), at the same driving voltage, the current of each PeLED fabricated using the mixed solvent was smaller than that of the PeLED fabricated using DMF solvent, which indicates the suppression of leakage current because of the coverage improvement of the $MAPbBr_3$ layer by the mixed solvent. As shown in Fig. 4(b), the luminance property of the PeLEDs was enhanced significantly by

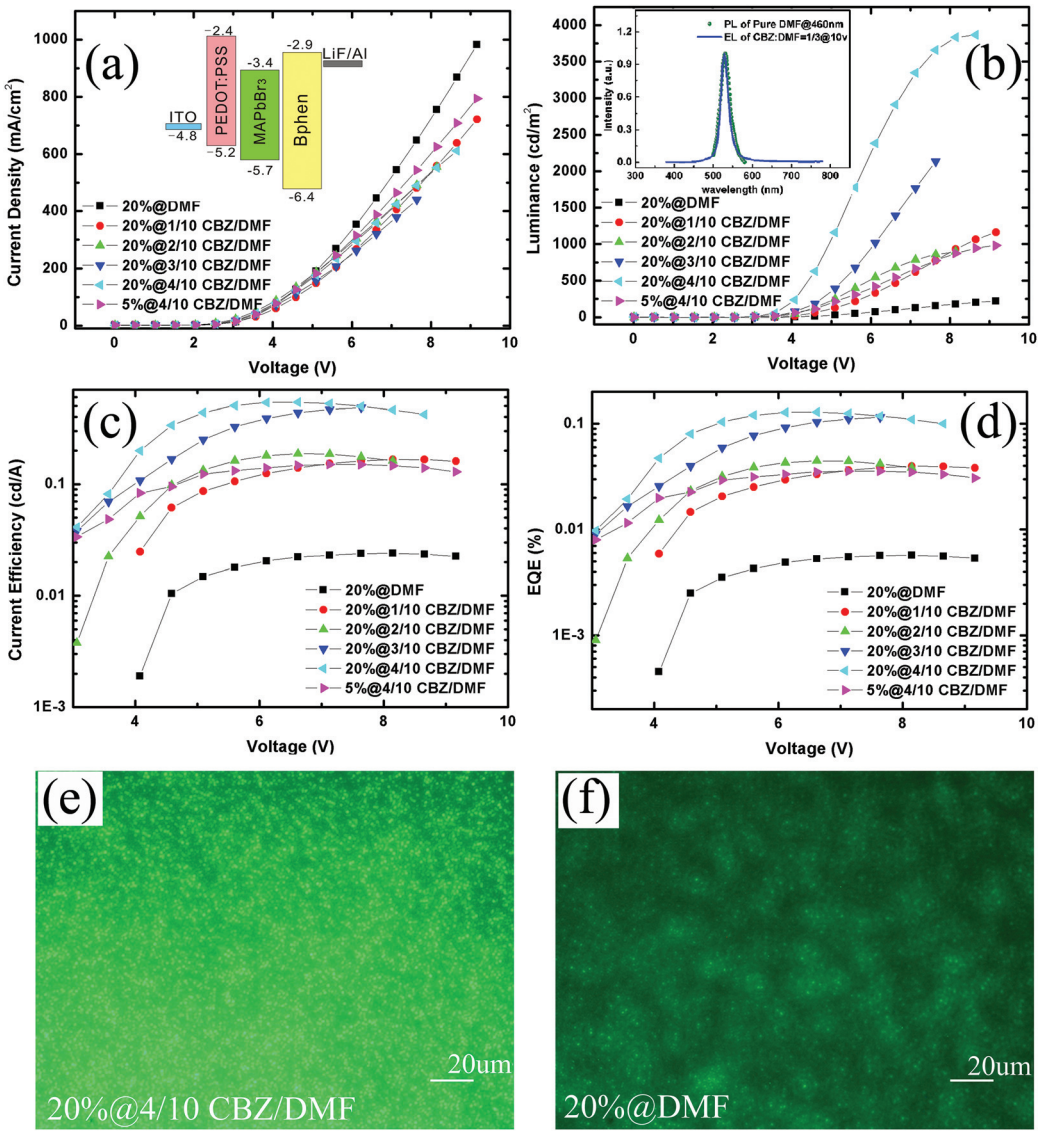

Fig. 4 (a) *J*–*V* and (b) *L*–*V* characteristics of PeLEDs fabricated using different solutions, respectively. Inset of (a): the energy level diagram of the PeLEDs. The energy level values were taken from the literature.[15,25] Inset of (b): normalized PL spectrum and normalized EL spectrum. (c) CE and (d) EQE performances for the PeLEDs. Microscope images of emission at 8 V for devices fabricated using a mixed solvent (e) and by using DMF solvent (f) are also shown.

using the mixed solvent. The PeLED fabricated using the 20 wt % $MAPbBr_3$/(CBZ/DMF = 4/10) solution exhibited the highest luminance among these devices, of 3846 cd m^{-2} at 8.6 V, which is about 19 times as bright as that of the control PeLED fabricated using the 20 wt% $MAPbBr_3$/DMF solution, which exhibited a luminance of 201 cd m^{-2} at 8.6 V. The turn-on voltages (driving voltage at 1 cd m^{-2}) for the PeLEDs based on different $MAPbBr_3$ films were all around 3.2 V, which demonstrates their potential application in low driving voltage light-emitting devices. The PL spectra of the $MAPbBr_3$ films, as well as the EL spectra of the PeLEDs, do not rely on the CBZ/DMF ratio. Typical EL and PL spectra are shown in the inset of Fig. 4(b). A strong green EL, centered at 528 nm and with a narrow full-width at half-maximum (FWHM) of 21 nm, could be measured, which is slightly blueshifted from the PL of the $MAPbBr_3$ film, centered at 531 nm and with an FWHM of 28 nm. Therefore, it can be confirmed that the light emission of the PeLEDs originates from the $MAPbBr_3$ layer.

Fig. 4(c) shows the current efficiency (CE) performance of the PeLEDs fabricated with different solutions. By assuming a Lambertian emission profile of the PeLEDs, their external quantum efficiency (EQE) performance was calculated and is shown in Fig. 4(d). As shown in Fig. 4(c) and (d), with the increase of CBZ addition, the devices showed a clear increase in CE and EQE. In particular, the PeLED prepared using 20 wt% $MAPbBr_3$/(CBZ/DMF = 4/10) solution exhibited the best performance. Its peak CE and EQE values were 0.54 cd A^{-1} and 0.13% respectively, which are about 22 times those of the control device fabricated with DMF solvent, the peak CE value and EQE value of which were 0.024 cd A^{-1} and 0.0057%, respectively. It has also been found that a higher solution concentration is important for the performance of the PeLEDs. As shown in Fig. 4(c) and (d), the performance of the PeLED fabricated using the low concentration (5 wt%) mixed solution was rather poor. The peak CE and EQE values were only 0.15 cd A^{-1} and 0.036%, respectively.

Fig. 4(e) and (f) show microscope images of PeLEDs fabricated with a CBZ/DMF mixed solvent and with DMF, respectively. Because of the high efficiency of the PeLED prepared using the mixed solvent, at the same driving voltage of 8 V, brighter luminance could be observed. Furthermore, as shown in Fig. 4(e), uniform emission could be observed for the PeLED fabricated with the mixed solvent. However, as shown in Fig. 4(f), aggregate island-like emission was found for the PeLED fabricated using DMF, which echoes the report of Yu *et al.*[14] This result confirms that the uniformity of the emission region of PeLEDs can also be significantly enhanced by the improved one-step solution process.

The influence of the mixed solvent on the luminescence properties of the $MAPbBr_3$ films was investigated by steady-state PL measurements. $MAPbBr_3$ films prepared using the DMF solution and the 1/4 CBZ/DMF solution were prepared for the test. As is shown in the inset of Fig. 5, the $MAPbBr_3$ film fabricated with the mixed solvent had a ~1.2 times increase in PL intensity compared with that of the film fabricated using DMF. The PL intensity enhancement induced by

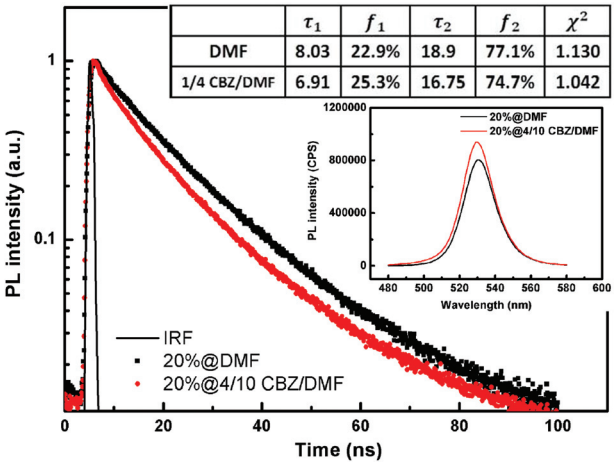

	τ_1	f_1	τ_2	f_2	χ^2
DMF	8.03	22.9%	18.9	77.1%	1.130
1/4 CBZ/DMF	6.91	25.3%	16.75	74.7%	1.042

Fig. 5 PL lifetime curves and steady-state PL spectra (inset) of $MAPbBr_3$ films fabricated using the DMF solution and the 1/4 CBZ/DMF solution. The black line is the instrument response function (IRF). The fast PL lifetime (τ_1) and the slow PL lifetime (τ_2), which were fitted by a biexponential decay model, are also shown in the inset.

the mixed solvent, however, was significantly smaller than the enhancement in the EL performance of the PeLED fabricated with the mixed solvent, which indicates that the excellent performance of the PeLED fabricated using the mixed solvent mainly benefits from the suppression of useless leakage current by the improved film morphology.

PL lifetime measurements were also conducted to further understand the PL performance of the films, as shown in Fig. 5. PL decay curves were fitted with a biexponential decay model as follows:

$$I = f_1 e^{-\frac{t}{\tau_1}} + f_2 e^{-\frac{t}{\tau_2}}, \quad (3)$$

where I is the normalized PL intensity, τ_1 and τ_2 are the lifetime of two decay components and f_1 and f_2 are the fractions of the two decay components. The fitted values are shown in the inset of Fig. 5. The two χ^2 values are close to 1, which indicates that the fitting results meet the tested results very well. According to the fitting results, the PL lifetime of the $MAPbBr_2$ is considered as the summation of fast- and slow-decay components, which is characterized by a short lifetime τ_1 and a long lifetime τ_2. The fast decay is related to trap-assisted recombination at grain boundaries, which is typically a non-radiative process, whereas the slow decay is related to radiative recombination inside the grains. Typically, a shorter lifetime indicates the acceleration of the corresponding recombination process. According to the fitted results, the film fabricated using the mixed solvent exhibits a shorter τ_2. Thus, the radiative recombination process of the film is accelerated, which indicates a stronger PL intensity. A possible reason for the decreased τ_2 is the decrease of crystal size by mixed solvent fabrication, which will limit the diffusion of excitons. However, the decrease of crystal size, as well as the increase of nucleation density, will also increase the grain boundaries,

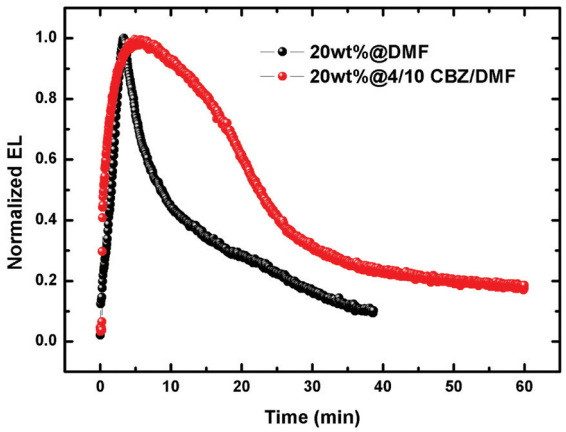

Fig. 6 The aging process at a constant current of 40 mA cm^{-2} for PeLEDs fabricated using 4/10 CBZ/DMF solution and by using DMF solution.

which will further enhance the trap-assisted non-radiative process and lead to a decrease of the short lifetime τ_1, just as shown in the inset of Fig. 5. Hence, the enhancement of the steady-state PL intensity of the film fabricated using the mixed solvent is the result of competition between the enhanced radiative recombination inside the grains and the enhanced trap-assisted recombination at grain boundaries.

Fig. 6 shows the aging process of PeLEDs fabricated using 20 wt% $MAPbBr_3$/(CBZ/DMF = 4/10) solution and by using 20 wt% $MAPbBr_3$/DMF solution. As shown in Fig. 6, the aging process of a PeLED can be divided into two distinctly separate time scales, with an early rapid decay process, followed by a slower decay process. For the control device fabricated by DMF, the rapid decay process lasted about 10 min, and a 50% signal drop was observed after 8 minutes. However, for the PeLED based on the mixed solvent, a rather slow aging process was observed. The rapid decay process lasted about 25 minutes, and a 50% signal drop was observed after 22 minutes. Since the $MAPbBr_3$ film could be stored in a glove box for more than 24 hours without any change in the photoluminescence and absorption properties, the rapid aging process of the PeLED cannot be attributed to the intrinsic decay of the $MAPbBr_3$ film. Furthermore, the improved ageing process for the PeLED fabricated using the mixed solvent indicates that morphological control is an effective way to enhance the PeLED stability. However, a detailed study is still needed for further understanding of the aging process of the PeLEDs.

Conclusions

In summary, a facile one-step solution process *via* a CBZ/DMF mixture to achieve controlled morphology of $MAPbBr_3$ films has been demonstrated. It was found that the coverage and the smoothness of the $MAPbBr_3$ films strongly depended on the proportion of CBZ in the mixture. Based on this improved solution process, an efficient green emission PeLED with a maximum luminance of 3846 cd m^{-2} and a maximum CE of 0.54 cd A^{-1} (EQE of 0.13%), which is 22 times higher than that of a device fabricated by a traditional one-step solution process, was demonstrated. Furthermore, this improved one-step solution process also benefits the uniformity of the emission region, as well as the stability performance of the PeLEDs. Our work demonstrates a facile and effective method for the morphological control of thin perovskite films, which will benefit the development of high-performance PeLEDs.

Acknowledgements

We acknowledge Dr Jinyan Zhao for the assistance of AFM measurements and Dr Xiaolong Yang for the assistance of the time-resolved PL spectrum measurements. This work has been supported by Basic Research Program of China (2013CB328705), National Natural Science Foundation of China (Grant No. 11574248, 61275034, 61106123), Ph.D. Programs Foundation of Ministry of Education of China (Grant No. 20130201110065), and International Cooperation by Shaanxi (Grant No. 2015KW-008). The SEM was measured at the International Centre for Dielectric Research (ICDR), Xi'an Jiaotong University.

Notes and references

1 D. B. Mitzi, K. Chondroudis and C. R. Kagan, *J. Res. Dev.*, 2001, **45**, 29–45.
2 Q. Chen, N. De Marco, Y. Yang, T.-B. Song, C.-C. Chen, H. Zhao, Z. Hong and H. Zhou, *Nano Today*, 2015, **10**, 355–396.
3 Y. Mei, C. Zhang, Z. V. Vardeny and O. D. Jurchescu, *MRS Commun.*, 2015, **5**, 297–301.
4 F. Deschler, M. Price, S. Pathak, L. E. Klintberg, D.-D. Jarausch, R. Higler, S. Huettner, T. Leijtens, S. D. Stranks, H. J. Snaith, M. Atatuere, R. T. Phillips and R. H. Friend, *J. Phys. Chem. Lett.*, 2014, **5**, 1421–1426.
5 Y.-H. Kim, H. Cho, J. H. Heo, T.-S. Kim, N. Myoung, C.-L. Lee, S. H. Im and T.-W. Lee, *Adv. Mater.*, 2015, **27**, 1248–1254.
6 G. Xing, N. Mathews, S. Sun, S. S. Lim, Y. M. Lam, M. Graetzel, S. Mhaisalkar and T. C. Sum, *Science*, 2013, **342**, 344–347.
7 M. Era, S. Morimoto, T. Tsutsui and S. Saito, *Appl. Phys. Lett.*, 1994, **65**, 676–678.
8 K. Chondroudis and D. B. Mitzi, *Chem. Mater.*, 1999, **11**, 3028–3030.
9 A. Kojima, K. Teshima, Y. Shirai and T. Miyasaka, *J. Am. Chem. Soc.*, 2009, **131**, 6050–6051.
10 M. M. Lee, J. Teuscher, T. Miyasaka, T. N. Murakami and H. J. Snaith, *Science*, 2012, **338**, 643–647.
11 H. Zhou, Q. Chen, G. Li, S. Luo, T.-b. Song, H.-S. Duan, Z. Hong, J. You, Y. Liu and Y. Yang, *Science*, 2014, **345**, 542–546.

12 Z.-K. Tan, R. S. Moghaddam, M. L. Lai, P. Docampo, R. Higler, F. Deschler, M. Price, A. Sadhanala, L. M. Pazos, D. Credgington, F. Hanusch, T. Bein, H. J. Snaith and R. H. Friend, *Nat. Nanotechnol.*, 2014, **9**, 687–692.
13 N. K. Kumawat, A. Dey, K. L. Narasimhan and D. Kabra, *ACS Photonics*, 2015, **2**, 349–354.
14 J. C. Yu, D. B. Kim, G. Baek, B. R. Lee, E. D. Jung, S. Lee, J. H. Chu, D.-K. Lee, K. J. Choi, S. Cho and M. H. Song, *Adv. Mater.*, 2015, **27**, 3492–3500.
15 J. Wang, N. Wang, Y. Jin, J. Si, Z.-K. Tan, H. Du, L. Cheng, X. Dai, S. Bai, H. He, Z. Ye, M. L. Lai, R. H. Friend and W. Huang, *Adv. Mater.*, 2015, **27**, 2311–2316.
16 L. Gil-Escrig, G. Longo, A. Pertegas, C. Roldan-Carmona, A. Soriano, M. Sessolo and H. J. Bolink, *Chem. Commun.*, 2015, **51**, 569–571.
17 O. A. Jaramillo-Quintero, R. S. Sanchez, M. Rincon and I. Mora-Sero, *J. Phys. Chem. Lett.*, 2015, **6**, 1883–1890.
18 G. Li, Z.-K. Tan, D. Di, M. L. Lai, L. Jiang, J. H.-W. Lim, R. H. Friend and N. C. Greenham, *Nano Lett.*, 2015, **15**, 2640–2644.
19 H. C. Cho, S. H. Jeong, M. H. Park, Y. H. Kim, C. Wolf, C. L. Lee, J. H. Heo, A. Sadhanala, N. Myoung, S. Yoo, S. H. Im, R. H. Friend and T. W. Lee, *Science*, 2015, **350**, 1222–1225.
20 K. Zheng, Q. Zhu, M. Abdellah, M. E. Messing, W. Zhang, A. Generalov, Y. Niu, L. Ribaud, S. E. Canton and T. Pullerits, *J. Phys. Chem. Lett.*, 2015, **6**, 2969–2975.
21 E. Baka, J. E. A. Comer and K. Takacs-Novak, *J. Pharm. Biomed. Anal.*, 2008, **46**, 335–341.
22 C. M. Pina and A. Putnis, *Geochim. Cosmochim. Acta*, 2002, **66**, 185–192.
23 D. Kashchiev and G. M. van Rosmalen, *Cryst. Res. Technol.*, 2003, **38**, 555–574.
24 D. Priante, I. Dursun, M. S. Alias, D. Shi, V. A. Melnikov, T. K. Ng, O. F. Mohammed, O. M. Bakr and B. S. Ooi, *Appl. Phys. Lett.*, 2015, 106.
25 M. Y. Chan, C. S. Lee, S. L. Lai, M. K. Fung, F. L. Wong, H. Y. Sun, K. M. Lau and S. T. Lee, *J. Appl. Phys.*, 2006, **100**, 094506.

